

# Effective model for in-medium $\bar{K}N$ interactions including the $L = 1$ partial wave

Aleš Cieplý<sup>1\*</sup>

*Nuclear Physics Institute, Academy of Sciences of the Czech Republic, Řež, Czech Republic*

Vojtěch Krejčířík<sup>2†</sup>

*Theoretical Research Division, RIKEN Nishina Center, Wako, Saitama, Japan*

## Abstract

Coupled channels model of meson-baryon interactions based on the effective chiral Lagrangian is extended to account explicitly for the  $\Sigma(1385)$  resonance that dominates the  $P$ -wave  $\bar{K}N$  and  $\pi\Sigma$  interactions at energies below the  $\bar{K}N$  threshold. The presented model aims at a uniform treatment of the  $\Lambda(1405)$  and  $\Sigma(1385)$  dynamics in the nuclear medium. We demonstrate the applicability of the model by confronting its predictions with the vacuum scattering data, then we follow with discussing the impact of nuclear matter on the  $\pi\Sigma$  mass spectrum and on the energy dependence of the  $K^-p$  branching ratios.

PACS numbers: 13.75.Jz, 14.20.Jn, 21.65.Jk

---

\* cieply@ujf.cas.cz

† vojtech.krejcirik@riken.jp

## I. INTRODUCTION

The low energy interactions of anti-kaons with nucleons represent a vital area where QCD, the quantum field theory of strong interactions, is tested in its nonperturbative region. For energies close to the threshold, the  $\bar{K}N$  interactions are dominated by the  $\Lambda(1405)$  and  $\Sigma(1385)$  resonances in the  $S$  and  $P$  waves, respectively. There, one often resorts to effective field theories [1], [2] combined with coupled channels resummation techniques [3], [4] to keep the QCD symmetries and overcome problems with convergence of the perturbative series in the presence of resonances. The sizable attraction existing between the anti-kaon and the nucleon is also relevant for a likely existence of the three-body  $K^-pp$  “molecular state” (see e.g. [5] and references there), for a formation of quasi-bound (anti)kaon-nuclear states [6], [7], or for a description of a hot and dense matter realized in heavy-ion collisions or in compact stars [8].

The nature and properties of strangeness  $S = -1$  baryon resonances are also very important issues in hadronic physics. The  $\Sigma(1385)$  with spin-parity  $J^P = 3/2^+$  is considered to belong to the baryon decuplet as a first excited state of  $\Sigma(1193)$  - this is in agreement with insight coming from the analysis of QCD in the limit of infinite number of colors [9], [10]. In the  $N_c \rightarrow \infty$  world, consistency relations [11], [12] require the decuplet of resonances involving  $\Sigma(1385)$  to be a part of a degenerate ground state multiplet together with the octet baryons. On the other hand the traditional quark picture has difficulty to accommodate the  $\Lambda(1405)$  ( $J^P = 1/2^+$ ) which is more likely a molecular  $\bar{K}N$  state rather than an excited three quarks state [13]. Currently, the most popular view is that  $\Lambda(1405)$  is generated dynamically as a  $\bar{K}N$  quasi-bound state submerged in  $\pi\Sigma$  continuum that provides another much broader resonance [14]. This picture emerges from coupled channels analysis with the inter-channel dynamics derived from an effective chiral Lagrangian. As a result one gets two resonant states close to the  $\bar{K}N$  threshold that are assigned to the  $\Lambda(1405)$  [15], [16]. The state at a higher energy, typically around 1420-1430 MeV, couples more strongly to the  $\bar{K}N$  channel and has a moderate width of 40-80 MeV, while the position of the other state is more model dependent and acquires a much broader width.

The formation of  $\Lambda(1405)$  has been a subject of several recent experiments aiming at establishing its structure. Provided the resonance is composed of two states, the observed mass spectra should depend on the reaction mechanism, particularly on involvement of either

$\pi\Sigma$  or  $\bar{K}N$  channels to which the two states couple with a different strength. Although this hypothesis explains the asymmetric shape of the  $\Lambda(1405)$  and generally is believed to be correct, the experimental results are still puzzling. The  $\Lambda(1405)$  signal in the  $pp \rightarrow Y^* + P + K^+$  reaction measured by the HADES collaboration at GSI [17] is compatible with the two-pole structure of the  $\Lambda(1405)$  as well as with the earlier measurement by the ANKE collaboration at COSY [18] or with the analysis of much older bubble chamber data from the  $\pi^-p$  experiments [19]. On the other hand, the  $\pi\Sigma$  mass spectra measured in a photoproduction reaction on a proton by the CLAS collaboration at JLab [20] have the  $I = 0$  peak at too low energy, close to the  $\pi\Sigma$  threshold. Nevertheless, the recent theoretical analyses [21], [22] seem to succeed at accommodating the data within the standard chirally motivated models. In addition two  $I = 1$  peaks were observed in the CLAS experiment at energies around 1400 MeV contributing to the enigmatic nature of the physics in the vicinity of the  $\Lambda(1405)$  resonance.

Another source of information on the  $\Lambda(1405)$  and  $\Sigma(1385)$  resonances should come from the studies of kaon-nuclear clusters by the AMADEUS experiment performed in Frascati [23]. As the preliminary data show, it is tricky to disentangle the contributions of the two excited hyperonic states when nuclear matter effects add up to other experimental uncertainties. Typically, the  $\Lambda(1405)$  mass spectra extracted from the  $\pi^\pm\Sigma^\mp$  distributions are contaminated by the  $\Sigma(1385)$  continuum. There, a theoretical model involving in-medium dynamics of both resonances treated in a uniform way might be of a vital help. In the present paper we aim at developing such model by using chirally motivated effective meson-baryon potentials that are constrained by the available experimental data on low-energy  $\bar{K}N$  interactions.

In the free space  $S$ -wave  $\bar{K}N$  and  $\pi\Sigma$  systems are reliably well described by chirally motivated coupled channels models that involve interactions of the  $J^P = 0^-$  meson octet with the  $J^P = 1/2^+$  baryon octet [3], [4], [16], [24], [25], [26], [27], [22]. Several authors have also extended the vacuum model to incorporate the influence of nuclear matter on the  $\bar{K}N$  system [28], [29], [30], [31], [32], [33]. It has been demonstrated that the dynamics of the  $\Lambda(1405)$  is responsible for switching the sign of the  $\bar{K}N$  scattering length from a negative value to a positive one at a relatively small density, about 1/10 of the typical nuclear density  $\rho_0 = 0.17 \text{ fm}^{-3}$  [34]. The  $K^-$ -nuclear interaction becomes even more attractive at subthreshold energies probed by kaonic atoms, though even larger attraction (most likely due to  $\bar{K}NN$  interactions) is needed to comply with phenomenological analysis of the experimental data

[33], [35]. A downside of these models, however, is that they are restricted only to the lowest partial wave  $L = 0$  leaving certain aspects of physics completely inaccessible—angular distribution of scattering cross section being the most obvious one. There were attempts to extend the approach to  $P$ -wave interactions in [36] and [37], and the first model was also used to study the properties of antikaons in nuclear matter [32]. Since the  $\Sigma(1385)$  is not generated dynamically [37], in the present paper we build on an already established  $S$ -wave model of Ref. [25] by adding the  $\Sigma(1385)$  resonance explicitly. As this resonance completely dominates the  $P$ -wave interactions around the  $\bar{K}N$  threshold an introduction of additional  $P$ -wave contributions does not seem necessary. With the model established to reproduce the available experimental data we then proceed to study the impact of nuclear medium on the shape of the  $\pi\Sigma$  mass spectra. In addition we also look at density and energy dependence of several  $K^-N$  branching ratios.

The paper is organized as follows. In section II, the general formalism of the spin 0 – spin 1/2 scattering is reviewed. The model itself is formulated in section III where its vacuum version as well as an extension to nuclear medium are presented. Our results and conclusions are discussed in sections IV and V, respectively.

## II. POTENTIAL SCATTERING FORMULATION

The main purpose of this section is to set the notation and introduce the terms and concepts related to the scattering of two particles, one of which has spin one-half and the other one is spinless (as is the case of meson-baryon scattering). The analysis presented here is restricted to interactions that are both time reversal and parity invariant. This loss of generality is fully justified since our ultimate goal is to understand processes governed by the strong interaction, i.e. the interaction that is invariant with respect to these symmetries. Additionally, throughout the paper only the first two partial waves ( $L = 0$  and  $L = 1$ ) are taken into account.

### A. General formalism of spin-zero spin-half scattering

The most general form of the scattering amplitude (recall that the same decomposition can be written down for the potential and, in general, for any quantity that is time reversal

and parity invariant) is a  $2 \times 2$  matrix in the spin space [38]:

$$F(\mathbf{p} \rightarrow \mathbf{p}') = \tilde{F}(\mathbf{p} \rightarrow \mathbf{p}') + i \boldsymbol{\sigma} \cdot \hat{\mathbf{p}} \times \hat{\mathbf{p}}' \tilde{G}(\mathbf{p} \rightarrow \mathbf{p}') . \quad (1)$$

Considering only the  $S$  and  $P$  partial waves, one obtains three independent components with well defined parity and total angular momentum:

- $L = 0, J = 1/2$  :  $0+$  partial wave,
- $L = 1, J = 1/2$  :  $1-$  partial wave,
- $L = 1, J = 3/2$  :  $1+$  partial wave.

The spin-flip ( $\tilde{G}$ ) and spin-non-flip ( $\tilde{F}$ ) amplitudes of Eq. (1) can be written in terms of the partial wave components as

$$\begin{aligned} \tilde{F} &= F^{0+} + (2F^{1+} + F^{1-}) \hat{\mathbf{p}} \cdot \hat{\mathbf{p}}' , \\ \tilde{G} &= F^{1+} - F^{1-} , \end{aligned} \quad (2)$$

where the hat indicates a unit vector in the respective direction. The general formula for the differential cross section with unpolarized beam and target is given as

$$\frac{d\sigma}{d\Omega}(\mathbf{p} \rightarrow \mathbf{p}') = |\tilde{F}(\mathbf{p} \rightarrow \mathbf{p}')|^2 + \sin^2(\theta) |\tilde{G}(\mathbf{p} \rightarrow \mathbf{p}')|^2 . \quad (3)$$

If only  $L = 0$  and  $L = 1$  are included — the case in which we are interested — the differential and total cross sections read:

$$\begin{aligned} \frac{d\sigma}{d\Omega} &= |F^{0+}|^2 + |2F^{1+} + F^{1-}|^2 \cos^2 \theta + |F^{1+} - F^{1-}|^2 \sin^2 \theta + \\ &\quad + (F^{0+}(2F^{1+} + F^{1-})^* + (F^{0+})^*(2F^{1+} + F^{1-})) \cos \theta , \end{aligned} \quad (4)$$

$$\sigma^{\text{tot}} = 4\pi \left( |F^{0+}|^2 + \frac{1}{3} |2F^{1+} + F^{1-}|^2 + \frac{2}{3} |F^{1+} - F^{1-}|^2 \right) . \quad (5)$$

The two-body potential obeying the desired symmetries (parity and time reversal) can be decomposed in exactly the same way — into three independent partial-wave components ( $V^{0+}$ ,  $V^{1+}$ , and  $V^{1-}$ ),

$$V = V^{0+} + (2V^{1+} + V^{1-}) \hat{\mathbf{p}} \cdot \hat{\mathbf{p}}' + (V^{1+} - V^{1-}) i \boldsymbol{\sigma} \cdot \hat{\mathbf{p}} \times \hat{\mathbf{p}}' . \quad (6)$$

In this scheme, the Lippmann-Schwinger equation for scattering amplitude splits into three independent equations — one for each partial wave ( $0+$ ,  $1-$ , and  $1+$ ) — with angular dependence fully determined by Eqs. (1), and (6):

$$F^{0+/1-/1+} = V^{0+/1-/1+} + V^{0+/1-/1+} G^{0/1} F^{0+/1-/1+} . \quad (7)$$

## B. The Lippmann-Schwinger equation with separable potentials

Considering only the  $S$  and  $P$  waves, there are three partial-wave effective potentials taken in the separable form, i.e.

$$\begin{aligned} V_{ij}^{0+}(p, p') &= g_i^0(p) v_{ij}^{0+} g_j^0(p'), \\ V_{ij}^{1-}(p, p') &= g_i^1(p) v_{ij}^{1-} g_j^1(p'), \\ V_{ij}^{1+}(p, p') &= g_i^1(p) v_{ij}^{1+} g_j^1(p'). \end{aligned} \tag{8}$$

The indexes  $i$  and  $j$  tag specific meson-baryon channels in the initial and final states, respectively, and  $g_j^L(p)$  stands for form factors in a given partial wave (and, in principle, for each scattering channel involved). They carry all the information about the incoming and outgoing momenta, more precisely about the absolute values of momenta, since the angular dependence has been factorized in the previous section. The form factors are taken in the Yamaguchi form [39], [40] as

$$g_j^0(p) = 1 / \left( 1 + \frac{p^2}{\alpha_j^2} \right), \tag{9}$$

$$g_j^1(p) = p / \left( 1 + \frac{p^2}{\alpha_j^2} \right)^{3/2}. \tag{10}$$

Here  $\alpha_j$  represents the inverse range parameter that is (in general) channel dependent. A concrete choice of form factors is arbitrary to a point. However, the Yamaguchi form for the  $S$ -wave (9) is widely used within the community and the form for  $P$ -wave (10) is its very natural extension. In particular, the form of  $g^1(p)$  is constrained by two requirements: first, the amplitude must satisfy a general low-momentum condition  $f = p^{2L+1} \cot(\delta)$  for  $p \rightarrow 0$  (this determines the linear dependence on  $p$ ); second, we want the convergence of the Green's functions in the Lippmann-Schwinger equation to be of the same order for both partial waves, i.e.  $g^0/g^1 \rightarrow \text{const.}$  when  $p \rightarrow \infty$  (this determines the power of the denominator in the  $g^1$  form). Let us note that the systematic error introduced at this point is compensated by the fact that the inverse ranges  $\alpha_j$  are free parameters of the model that will eventually be fitted to data.

The separable form of the potentials allows us to use the same ansatz for the scattering amplitudes as well,

$$\begin{aligned}
F_{ij}^{0+}(p, p') &= g_i^0(p) f_{ij}^{0+} g_j^0(p'), \\
F_{ij}^{1-}(p, p') &= g_i^1(p) f_{ij}^{1-} g_j^1(p'), \\
F_{ij}^{1+}(p, p') &= g_i^1(p) f_{ij}^{1+} g_j^1(p').
\end{aligned} \tag{11}$$

Then, the Lippmann-Schwinger equation is reduced into three algebraic equations,

$$\begin{aligned}
f_{ij}^{0+} &= \left[ (\mathbf{1} - v^{0+} \cdot G^0)^{-1} \cdot v^{0+} \right]_{ij}, \\
f_{ij}^{1-} &= \left[ (\mathbf{1} - v^{1-} \cdot G^1)^{-1} \cdot v^{1-} \right]_{ij}, \\
f_{ij}^{1+} &= \left[ (\mathbf{1} - v^{1+} \cdot G^1)^{-1} \cdot v^{1+} \right]_{ij},
\end{aligned} \tag{12}$$

where the Green functions are energy dependent diagonal matrices represented by the integrals

$$G_n^0(\sqrt{s}) = -\frac{1}{2\pi^2} \int d^3q \frac{[g^0(q)]^2}{p_n^2 - q^2 + i\epsilon} = \frac{\alpha}{2} \frac{\alpha^2}{(\alpha - ip_n)^2}, \tag{13}$$

$$G_n^1(\sqrt{s}) = -\frac{1}{2\pi^2} \int d^3q \frac{[g^1(q)]^2}{p_n^2 - q^2 + i\epsilon} = \frac{\alpha^3}{2} \frac{\alpha^2 (\alpha - 3ip_n)}{(\alpha - ip_n)^3}. \tag{14}$$

Here  $p_n$  denotes the on-shell meson-baryon CMS momenta in the  $n$ -th channel and the integration can be performed analytically in the free space.

### III. CHIRALLY AND COLORFULLY MOTIVATED POTENTIALS

In this section, the chiral and large  $N_c$  based model for the meson-baryon interactions in the strange sector that includes both  $S$ - and  $P$ -waves is formulated. Our aim is to extend the existing model of Ref. [25], which includes only the  $S$ -wave, to accommodate the  $P$ -wave physics as well.

The dynamics of the anti-kaon nucleon system is determined by the coupled channels potentials within the formalism presented in the previous section. We employ potentials that are motivated by the chiral  $SU(3)$  dynamics and comply with the large  $N_c$  consistency relations. For the  $L = 0$  part of our model we take the leading order Tomozawa-Weinberg (TW) interaction that is represented by potentials used successfully and discussed in detail in [25]. Here, we rather focus on the  $P$ -wave physics, the main novelty of the current work.

It is well known that the  $S$ -wave  $\Lambda(1405)$  resonance is generated dynamically already by the leading order TW interaction. On the other hand, the situation is principally different

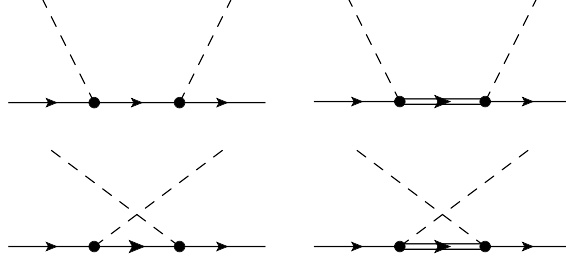


FIG. 1. Feynman diagrams representing leading order interactions in the  $P$ -wave sector.

in the  $L = 1$  sector, where the most significant contributions come from the direct and crossed Born diagrams. It was discussed in the preceding work [37] that considering only octet baryons in the intermediate state (left diagrams in Fig. 1), one is not able to reproduce the resonant behavior which could be identified as the  $\Sigma(1385)$ . Thus, in order to formulate a phenomenologically relevant model, one is forced to include the decuplet baryons with the  $\Sigma(1385)$  being one of them, as building blocks as well (right diagrams in Fig. 1). We recall that this situation (treating both octet and decuplet baryons in the same way) is analogous to the one which occurs in the large  $N_c$  limit of QCD. There, the consistency relations [11], [12], [41], [42], [43], [44] require the octet and decuplet baryons to be degenerate and form a ground state multiplet of the contracted  $SU(2N_f)$  symmetry. It seems natural to take inspiration from this idea when designing the  $P$ -wave part of our model.

Having decuplet baryons as fundamental degrees of freedom, one can construct four different diagrams contributing in the leading order: a direct one with the octet baryon in the intermediate state, a direct one with the decuplet baryon in the intermediate state, a crossed one with the octet baryon in the intermediate state, and a crossed one with the decuplet baryon in the intermediate state. These four possibilities are depicted in Fig. 1.

In general, the meson-baryon-baryon vertex is of the form

$$\frac{\partial^i \phi^a}{f_\pi} \langle B' | \sigma^i \lambda^a | B \rangle \sim X^{ia}, \quad (15)$$

where the  $X^{ia}$  stands for a generalized spin-flavor operator acting on the baryon ground state multiplet [43], [44]. It represents a straightforward generalization of a  $\sigma^i \tau^i$  Pauli matrix product standing at a standard pion-nucleon vertex. This operator is strongly constrained by the emergent spin-flavor symmetry at large  $N_c$ . Specifically, the relative strengths of the couplings are determined by appropriate Clebsch-Gordan coefficients of  $SU(2)$ -spin and  $SU(3)$ -flavor group,



$$\Gamma \sim (\text{baryonIN}, \text{mesonIN} | \text{baryonOUT})_{SU(2)\text{-spin}} \\ (\text{baryonIN}, \text{mesonIN} | \text{baryonOUT})_{SU(3)\text{-flavor}} , \quad (16)$$

and the absolute strengths are fixed to obey the the large  $N_c$  consistency relations. The relevant  $SU(3)$ -flavor Clebsch-Gordan coefficients as well as absolute strengths of the couplings are discussed in detail in the Appendix, and the coupling matrices for the  $SU(2)$ -spin transitions can be found in [45].

Let us note that even though we use the large  $N_c$  limit to motivate the model, the Clebsch-Gordan coefficients for  $SU(3)$ -flavor group considered in this paper correspond to  $N_c = 3$  [46], [47]. The reason for this is a practical one, particularly because the Clebsch-Gordan coefficients including states with strangeness are suppressed as  $N_c \rightarrow \infty$  thus leading to a trivial interaction.

### A. Free space potential

The construction of the  $S$ -wave effective potential by matching it to the chiral meson-baryon amplitude is well documented in the literature [3], [4], [25]. For the  $0^+$  partial wave, the leading order contribution comes from the Tomozawa-Weinberg term which we take in a form

$$V_{ij}^{TW}(p, p') = -\frac{1}{4\pi f_\pi^2} \sqrt{\frac{M_i M_j}{s}} \left[ -\frac{1}{4} \mathcal{C}^{TW} (\sqrt{s} - M_i - M_j) \right] . \quad (17)$$

In the present work it is the only potential contribution we consider in the  $S$ -wave and since it bears no angular dependence,  $V_{ij}^{TW}(p, p')$  is also equal to  $v_{ij}^{0+}$ . The strength of the interchannel couplings is determined by the  $\mathcal{C}^{TW}$  matrix which is given by the standard  $SU(3)$  Clebsch-Gordan coefficients. In principle, the potential (17) should be complemented by contributions that represent higher orders in the chiral expansion, and by the direct and crossed Born diagrams. However, since we concentrate on the impact of the  $P$ -wave and on in-medium applications we prefer to keep the meson-baryon potential as simple as possible and leave a further refinement of our model for a future.

In the  $P$ -wave sector, it is straightforward to determine which of the four leading-order diagrams shown in Fig. 1 plays a key role in the energy region of interest. Due to a suppression in the energy denominator caused by the necessity to excite the incoming baryon, the

dominant contribution comes from the direct Born term with the decuplet in the intermediate state. For the strangeness-isospin combination discussed in this study, the intermediate baryon is the  $\Sigma(1385)$ . Thus, our  $P$ -wave potential can be written as

$$V_{ij}(p, p') = -\frac{1}{4\pi f_\pi^2} \sqrt{\frac{M_i M_j}{s}} \mathcal{C}_{\Sigma^*0}^{d10} \left( -\frac{\sqrt{2}}{\sqrt{s} - \tilde{M}_{\Sigma^*0}} \mathbf{p} \cdot \mathbf{p}' - \frac{\frac{1}{\sqrt{2}}}{\sqrt{s} - \tilde{M}_{\Sigma^*0}} i \boldsymbol{\sigma} \cdot \mathbf{p} \times \mathbf{p}' \right), \quad (18)$$

where  $\tilde{M}_{\Sigma^*0}$  represents the bare  $\Sigma(1385)$  mass. From here, one immediately obtains the relevant partial wave component that enters the Lippmann-Schwinger equation (12),

$$v_{ij}^{1,+} = -\frac{1}{4\pi f_\pi^2} \sqrt{\frac{M_i M_j}{s}} \left( -\frac{1}{\sqrt{2}} \mathcal{C}_{\Sigma^*0}^{d10} \frac{1}{\sqrt{s} - \tilde{M}_{\Sigma^*0}} \right). \quad (19)$$

The coupling matrix  $\mathcal{C}_{\Sigma^*0}^{d10}$  is determined by the  $SU(3)$ -flavor Clebsch-Gordan coefficients and large  $N_c$  consistency relations following our motivation at the beginning of this section. The exact specification of the  $\mathcal{C}_{\Sigma^*0}^{d10}$  matrix is relayed to the Appendix. We also note that restricting our  $P$ -wave only to the excitation of  $\Sigma^*$ , which has a total angular momentum 3/2, implies that the partial wave potential component  $v^{1-}$  is identically zero.

## B. In-medium extension

As mentioned in Section I and already tested in several applications restricted to the  $S$ -wave sector, the separable potential model is well suited to study the impacts of nuclear matter on meson-baryon interactions. The analysis of nuclear-medium effects on the full model (including the  $P$ -wave) is presented in this section.

In principle, the nuclear medium affects the meson-baryon system in two ways. Firstly, for the channels involving nucleons the Pauli principle restricts the available phase-space which effectively shifts the respective intermediate state threshold to higher energies. Secondly, the interacting hadrons acquire self-energies due to their interaction with nuclear matter which shifts the position of the pole in the intermediate state propagator. For the  $\bar{K}N$  system both effects compensate each other to a large extent [33]. The Pauli blocking moves the  $\Lambda(1405)$  structure above the  $\bar{K}N$  threshold where the resonance is partly dissolved [28], but the inclusion of nucleon and kaon self-energies [29] brings it back below the threshold, though the  $\bar{K}N$  related pole apparently moves to a more distant Riemann sheet.

When implementing the nuclear medium effects we follow the procedure adopted in Refs. [25] and [33]. The intermediate state meson-baryon Green function of Eqs. (13) and

(14) is then modified as:

$$G_n^L(\sqrt{s}, \rho) = -4\pi \int_{\Omega_n(\rho)} \frac{d^3q}{(2\pi)^3} \frac{[g_n^L(q^2)]^2}{p_n^2 - q^2 - \Pi_n(\sqrt{s}, \rho) + i\epsilon}, \quad (20)$$

with  $\Pi_n(\sqrt{s}, \rho)$  standing for the sum of the meson and baryon self-energies [31]. The integration is carried over the  $\Omega_n(\rho)$  domain of momenta allowed by the Pauli principle (intermediate state nucleon momenta above the Fermi limit) [28]. In such situation, the integral in Eq. (20) is to be evaluated numerically. We also note that not only the Green function (20) but also the amplitudes  $f_{ij}$  that one gets by solving Eqs. (12) become density dependent quantities.

To simplify the matters we consider the nucleons at rest when evaluating the domain  $\Omega_n(\rho)$ , neglecting completely the influence of their Fermi motion. With the exception of kaons that are treated selfconsistently we also assume a simple energy independent form for the hadron self-energies

$$\Pi_n^h(\rho) = 2\mu_n V_0^h \rho / \rho_0, \quad (21)$$

where  $h$  tags the specific particle (either meson or baryon) and  $\mu_n$  is the relativistic meson-baryon reduced energy. For the baryons we take  $V_0^\Lambda = (-30 - i10)$  MeV,  $V_0^\Sigma = (30 - i10)$  MeV and  $V_0^N = (-60 - i10)$  MeV, for the optical potential depths, the values that are consistent with mean-field potentials used in nuclear structure calculations and were already tested in previous  $\bar{K}$ -nuclear and  $\eta$ -nuclear calculations [33], [48]. The imaginary parts of the baryon optical potentials reflect a possibility of the inelastic hadron-nuclear processes as well as of the  $\Sigma N \rightarrow \Lambda N$  conversion. The uniformly adopted value of  $\Im V_0 = -10$  MeV represents a fair estimate for all three hadrons with any anticipated corrections falling below the overall level of theoretical ambiguities present in our model. We also note in passing that the self-energies that enter Eq. (20) differ by a kinematic factor  $\mu_n/E_h$  (with  $E_h$  denoting the hadron energy in the meson baryon CMS) from the self-energies used in the equation of motion written in the laboratory frame where the nuclear matter is at rest.

The evaluation of the pion optical potential depth  $V_0^\pi$  at energies in a vicinity of the  $\Delta(1232)$  resonance represents a delicate issue. There, the  $\pi N$  interaction changes from attractive below the resonance to repulsive at energies above the resonance. For the  $\pi\Sigma$  CMS energies below the  $\bar{K}N$  threshold the pion momenta are about 130 – 180 MeV in the LAB system with nuclear matter at rest. This relates to the  $\pi N$  CMS energies below the  $\Delta(1232)$  resonance, where the pion-nuclear optical potential is attractive and few tens

of MeV deep at central nuclear density [49]. However, when the Fermi motion and other nuclear medium effects are considered, it is clear that our interactions cover a broad region of  $\pi N$  energies below and above the  $\Delta(1232)$  resonance. Thus, it is feasible to approximate the pion optical potential with a purely imaginary value of  $V_0^\pi$ . The later quantity can be estimated by using a relation

$$2\mu_{\pi N} \Im V_0^\pi(\sqrt{s}) = -4\pi \Im F_{\pi N}(\sqrt{s}, 0^\circ) \rho_0 = -p_{\pi N} \sigma_{\pi N}(\sqrt{s}) \rho_0 \quad (22)$$

where  $F_{\pi N}(\sqrt{s}, 0^\circ)$  represents a forward free space scattering amplitude and  $\sigma_{\pi N}$  stands for the total pion-nucleon cross section. At the energies related to our work the SAID database [50] provide the  $F_{\pi N}$  amplitudes (or cross sections) that result into  $\Im V_0^\pi$  values from  $-10$  to  $-50$  MeV. For the purpose of our analysis, we have decided to go with  $V_0^\pi = -i30$  MeV, a value consistent with the phenomenological potentials reported in Refs. [49], [51].

Finally, the (anti)kaon optical potential is standardly constructed as a coherent sum of one-nucleon contributions which leads to the selfenergy

$$\Pi^{\bar{K}} = -4\pi F_{\bar{K}N} \rho. \quad (23)$$

Since this self-energy is expressed through the  $\bar{K}N$  amplitudes that are obtained as a solution of the Lipmann-Schwinger equations (12) the coupled channels system of equations has to be solved iteratively to achieve selfconsistency, see Refs. [31], and [33] for details. Standardly, only 5-7 iterations are sufficient in the procedure.

#### IV. FREE SPACE AND IN-MEDIUM RESULTS

The effective potential constructed in previous section contains several free parameters that can be fixed in fits to low energy  $K^-p$  data. Here we adopt an already established TW1 parametrization of [25] for the  $0+$  potential with only one inverse range used in all channels,  $\alpha_j = \alpha = 701$  MeV, and with the meson decay constant  $f_\pi = 113$  MeV. With this simple setting one gets quite satisfactory description of all available low energy  $K^-p$  data including the characteristics of kaonic hydrogen [25].

Concerning the the  $P$ -wave potential (19) we note that it contains no additional free parameter as the bare value of  $\Sigma(1385)$  baryon mass is to be adjusted in a way that the position of the  $\Sigma(1385)$  resonance is well reproduced. By doing so we got  $\tilde{M}_{\Sigma^*0} = 1590$

MeV. The relatively large difference between the bare and the physical mass of the  $\Sigma(1385)$  resonance is due to the fact that the pole shift is closely correlated to the value of the inverse range parameter  $\alpha$ . Since it was our intention to have a fully fixed P-wave model, we decided to use the value of  $\alpha$  determined in the preceding analysis. We prefer this approach to fixing either  $\alpha$  or  $\tilde{M}_{\Sigma^*0}$  at some arbitrary point as well as to performing an additional fit of these values to the experimental data that we aim to predict.

With all parameters of our effective anti-kaon nucleon model fixed we demonstrate its ability to reproduce the available  $K^-p$  reactions data at low energies. The total cross sections for the  $K^-p$  scattering into various channels are shown in Fig. 2. One can clearly see that the  $S$ -wave contribution dominates the total cross section in the whole energy region considered (up to 300 MeV kaon momentum). This observation is in agreement with a naive expectation that the  $L = 1$  partial wave contribution is small at energies considered in our analysis.

The physical quantity where  $P$ -wave physics plays a crucial role (and therefore can serve as an honest testing ground for the present model) is the angular distribution of the scattering cross section. In Figs. 3 and 4, the differential cross sections for the elastic and charge-exchange reactions are shown. It is nice to observe that values predicted by our model are in a very good agreement with the experimental data. The direction of the slope (increasing for the elastic and decreasing for the charge-exchange reactions) is unquestionably reproduced. The angle of the slope is slightly underestimated for  $K^-p \rightarrow K^-p$ , whereas for the  $K^-p \rightarrow \bar{K}^0n$  reaction it matches the experimental observation rather accurately. We also note that the data on the differential cross sections are far more accurate and consistent than the asymmetries used in the preceding work [37].

Finally, with all the ingredients in place, we use the model to study impacts of nuclear matter on the shape of  $\pi\Sigma$  mass distributions and on selected branching ratios that might be relevant for the analysis of the spectra measured experimentally. We start our analysis by demonstrating the nuclear medium effects on the  $\pi\Sigma$  amplitudes. The amplitudes are shown in Fig. 5 for the two discussed partial waves and isospins  $I = 0$  and  $I = 1$ . The left and right panels present the real and imaginary parts of the amplitudes, respectively. The isoscalar  $\pi\Sigma$   $P$ -wave amplitudes are omitted in our analysis as their impact on the discussed physical phenomena is negligible in the energy interval around the  $\bar{K}N$  threshold. We also disregard the isotensor part of the  $\pi\Sigma$  amplitude.

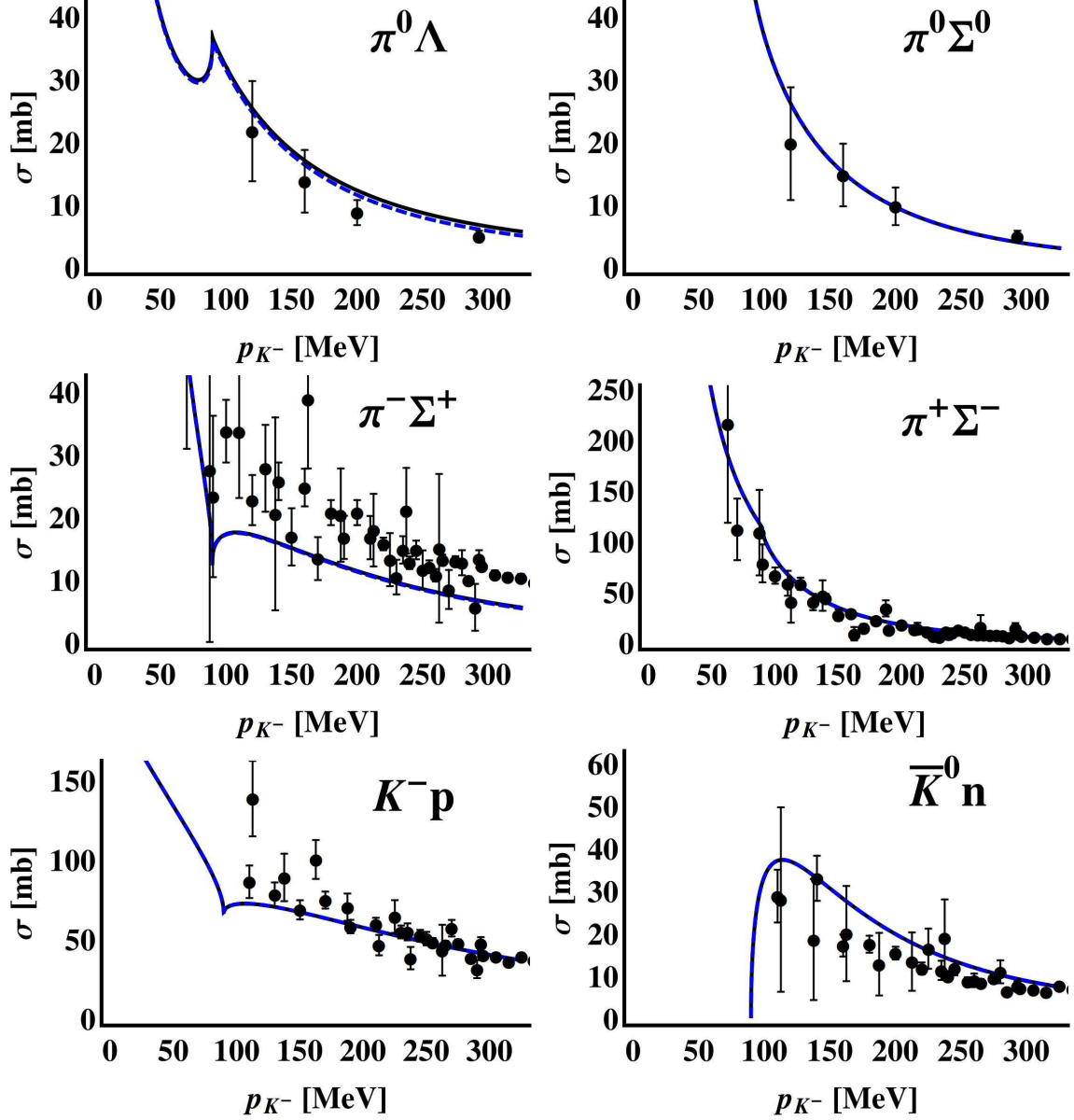


FIG. 2. Total  $K^-p$  cross sections for  $\pi^0\Lambda$ ,  $\pi^0\Sigma^0$ ,  $\pi^-\Sigma^+$ ,  $\pi^+\Sigma^-$ ,  $K^-p$ , and  $\bar{K}^0n$  channels (from the top left). Experimental data are from [52], [53], [54], [55], [56] [57], [58]. Full line represents the full model (S and P waves) whereas the dashed line corresponds to the TW1 model (only S wave).

The  $S$ -wave part of the isoscalar  $\pi\Sigma$  amplitude shown at the top panels of Fig. 5 clearly demonstrates the importance of the  $\Lambda(1405)$  resonance. At first, let us have a look at the lines that represent the free-space results. As the  $\pi\Sigma$  channel couples more strongly to the lower of the two  $I = 0$  poles generated by the model the peak in the imaginary part of the free-space amplitude is located below 1400 MeV. However, since the  $\pi\Sigma\text{-}\bar{K}N$  coupling

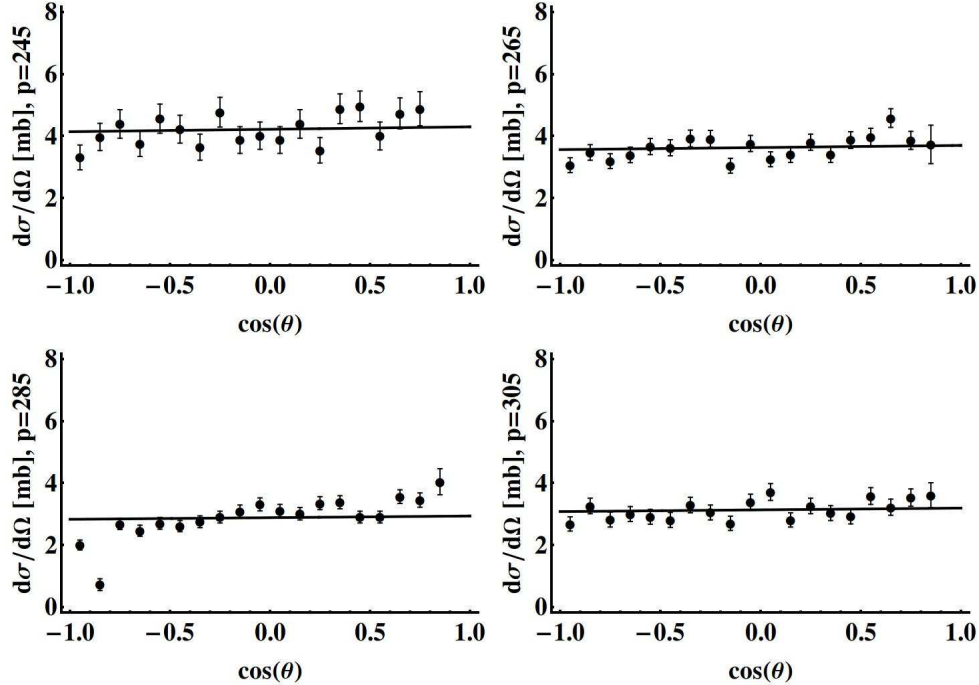


FIG. 3. Differential cross section for the  $K^-p \rightarrow K^-p$  reaction at various energies. Experimental data are from [56]. Theoretical curves are normalized so that the total cross section is equal to the experimental one.

is quite strong, the second pole (related to  $\bar{K}N$  quasibound state) has also an impact on the amplitude and results in the second sign reversal of the real part of the amplitude. Both points at which the real part of the amplitude crosses the zero axis relate reasonably well to the positions of the two poles assigned to the  $\Lambda(1405)$ . For the TW1 model used in the present work the poles are located at complex energies  $z_1 = (1371, -54)$  MeV and  $z_2 = (1433, -25)$  MeV. The effect of Pauli blocking imposed on the  $\pi\Sigma$  system is visualized by the dot-dashed lines in the figure. The resonance structure is moved to higher energies and partially dissolves in the nuclear matter. The additional inclusion of hadron selfenergies shown by the continuous lines moves the structure back to lower energies, about 20-30 MeV below the  $\bar{K}N$  threshold. Particularly, the nucleon self-energy is responsible for most of the shift with the other hadron self-energies having a moderate impact on the shape and width of the resonance. As far as the  $\bar{K}N$  related pole assigned to the  $\Lambda(1405)$  remains close to the real axis the resonance remains relatively narrow, interposed on the continuum formed by the second  $\pi\Sigma$  related pole and by the other involved channels. These results are quite in line with observations made for the  $\bar{K}N$  amplitudes in [25] and [33].

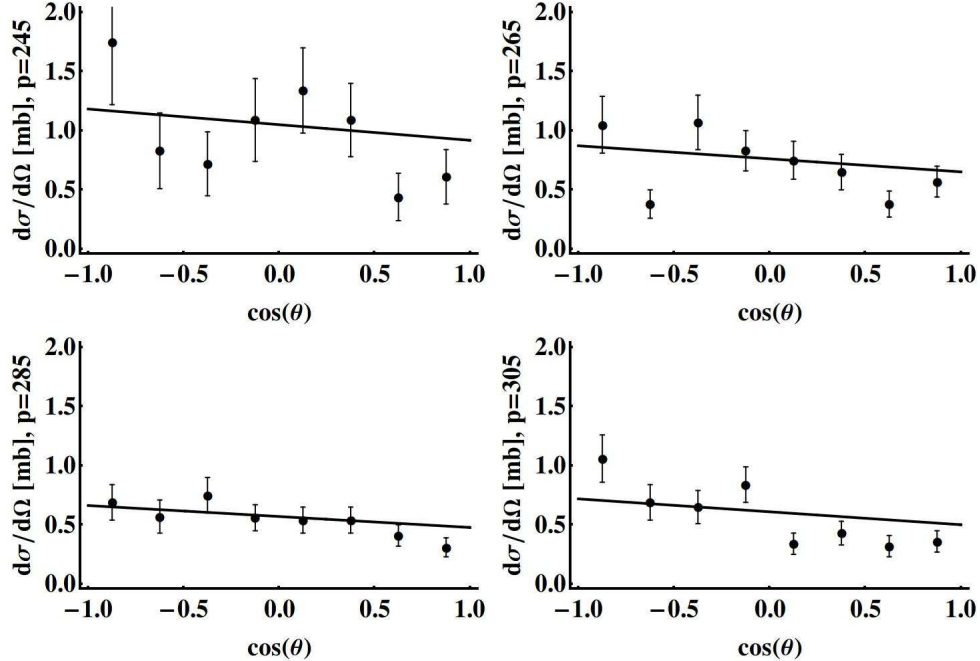


FIG. 4. Differential cross section for the  $K^-p \rightarrow \bar{K}^0n$  reaction at various energies. Experimental data are from [56]. Theoretical curves are normalized so that the total cross section is equal to the experimental one.

The  $S$ -wave part of the isovector  $\pi\Sigma$  amplitude is given in the middle panels of Fig. 5. Apparently, its magnitude is much smaller than the isoscalar one dominated by the presence of  $\Lambda(1405)$ . Still, a sharp peak at the  $\bar{K}N$  threshold observed in the imaginary part of the amplitude indicates a presence of a pole nearby. Such isovector pole was already reported in [15] and its existence was argued for in Refs. [25] and [33]. A possible existence of an isovector resonance close to the  $\bar{K}N$  threshold may also be supported by the new CLAS data on the  $\gamma p \rightarrow K^+\pi^\pm\Sigma^\mp$  reactions [20].

Finally, the bottom panels of Fig. 5 present our results for the  $P$ -wave part of the isovector  $\pi\Sigma$  amplitude. The imaginary part of the amplitude shows a resonance with a width of about 30 MeV, in a reasonable agreement with the  $\Sigma(1385)$  resonance width of 36 MeV listed by the Particle Data Group [59]. Unlike the  $S$ -wave amplitudes the Pauli blocking has little impact on the  $P$ -wave ones. We checked that the same applies to the  $P$ -wave part of the elastic  $\bar{K}N$  amplitude, so the observation does not apply exclusively to the  $\pi\Sigma$  channel. The feature is most likely related to our treatment of the  $P$ -wave interaction that is restricted to a formation of an intermediate  $\Sigma(1385)$  resonance, see Eq. (18). The inclusion of hadron



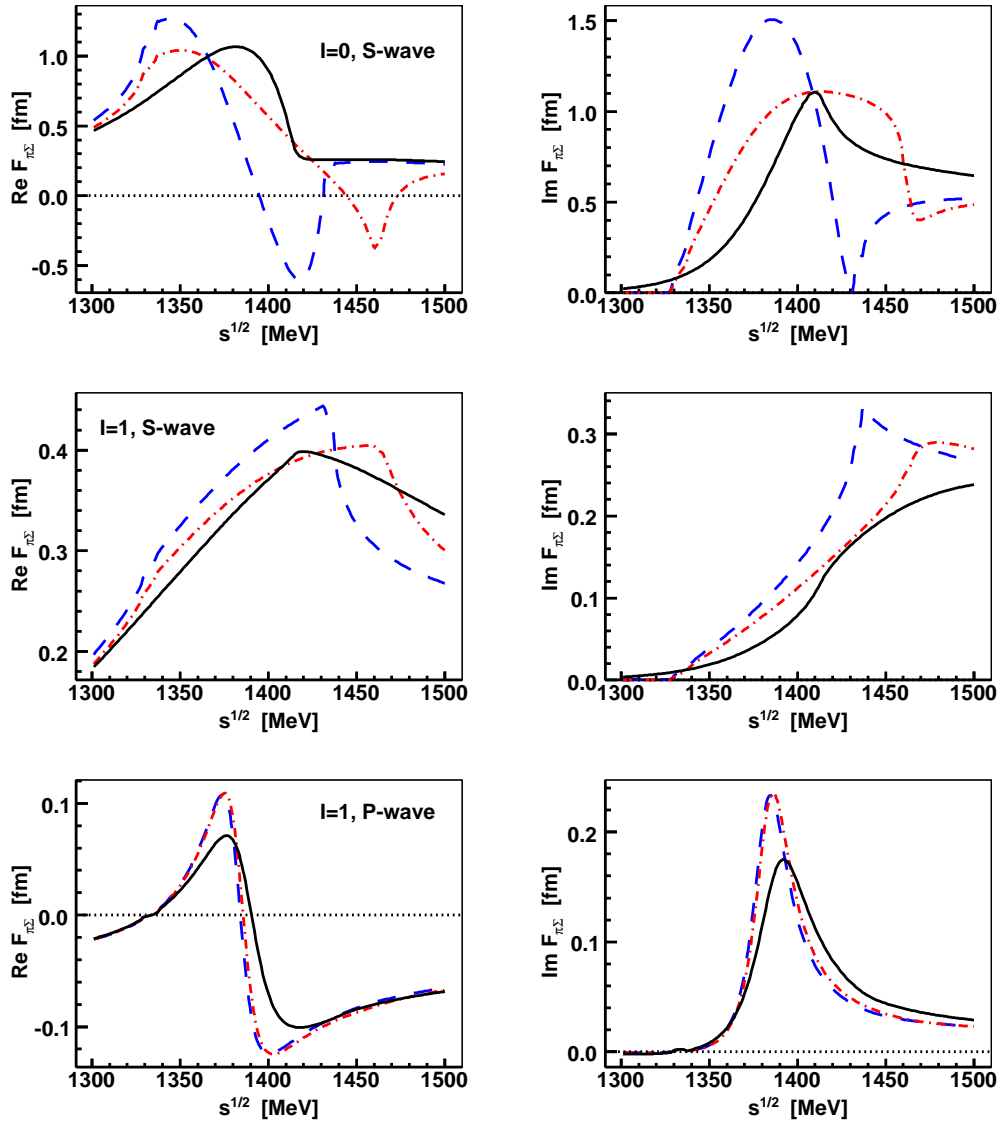


FIG. 5. Energy dependence of the  $\pi\Sigma$  amplitudes. The dashed (blue) lines show the free space results, the dot-dashed (red) and continuous lines demonstrate the effects of including Pauli blocking only and Pauli blocking together with hadron selfenergies, respectively.

self-energies practically does not affect the position of the resonance structure impacting only on the magnitude of the observed peak. Apparently, the leading resonant interaction in the Born term is much stronger than higher order contributions of the expansion that include intermediate meson-baryon states affected by the nuclear medium.

At this point we find it appropriate to mention the sensitivity of our in-medium results to the adopted form of the pion self-energy. The whole effect is demonstrated in Fig. 6 for the

same amplitudes as those in Fig. 5. The calculations were made for three different values of the purely imaginary pion-nuclear optical potential depth,  $iV_0^\pi = 10, 30$  and  $50$  MeV, and for the optical potential depth of  $V_0^\pi = (30 - i10)$  MeV used previously in Ref. [33]. As observed in the figure, a feasible increase of the imaginary part  $\Im V_0^\pi$  decreases the magnitude of the  $\Lambda(1405)$  resonance structure shown in the top panels. Similarly, a smaller pion-nuclear absorption leads to a more pronounced in-medium resonance. The same, though much smaller, effects are seen in the bottom panels where the  $\Sigma(1385)$  resonance structure is manifested. Interestingly, an addition of a repulsive nonzero real part to the pion-nuclear potential (as anticipated in [33]) does not have a significant impact on the position of the  $\Lambda(1405)$  and  $\Sigma(1385)$  structures, but the magnitude of both peaks gets increased. As there is no genuine peak in the in-medium isovector  $\pi\Sigma$  amplitude shown in the middle panels of the figure the variation of pion self-energy has a relatively small impact there. The results shown in Fig. 6 can also be viewed as a demonstration of theoretical ambiguities and a measure of anticipated theoretical errors in our predictions. We also note that our results obtained for the largest pion absorption,  $iV_0^\pi = 50$ , MeV are in a reasonable agreement with observations made in [32] where a more sophisticated formulation of the pion-nuclear optical potential was adopted. On the other hand the authors of [32] consider an unlikely  $\Sigma$ -nuclear attractive interaction in their model and it remains to be seen whether their treatment of in-medium pions based on particle-hole and  $\Delta$ -hole excitations is really a realistic one.

To complete the analysis of theoretical ambiguities we also checked the sensitivity of our results to the variations of (not so well established) imaginary parts of the baryon self-energies. We have found that neglecting completely the imaginary parts of the nucleon and  $\Lambda$  self-energies, or increasing the imaginary part of the  $\Sigma$  optical potential depth to  $\Im V_0^\Sigma = -i20$  MeV has marginal effect on the computed in-medium  $\pi\Sigma$  amplitudes.

We now turn our attention to the energy and density dependence of the branching ratio

$$\gamma_p = \frac{\sigma(K^-p \rightarrow \pi^+\Sigma^-)}{\sigma(K^-p \rightarrow \pi^-\Sigma^+)} = \frac{\Gamma(\pi^+\Sigma^-)}{\Gamma(\pi^-\Sigma^+)}, \quad (24)$$

where the expression utilizing the transition probabilities  $\Gamma(j) = 8\pi |F_{K^-p,j}|^2$  can be used even for energies below the  $K^-p$  threshold. The threshold value  $\gamma_p = 2.360 \pm 0.040$  [60] represents one of the experimental quantities fitted by the TW1 model. In Fig. 7 we show its energy dependence and how it is affected by the nuclear medium due to the Pauli blocking and hadron selfenergies when evaluating the intermediate state meson-baryon propagator.

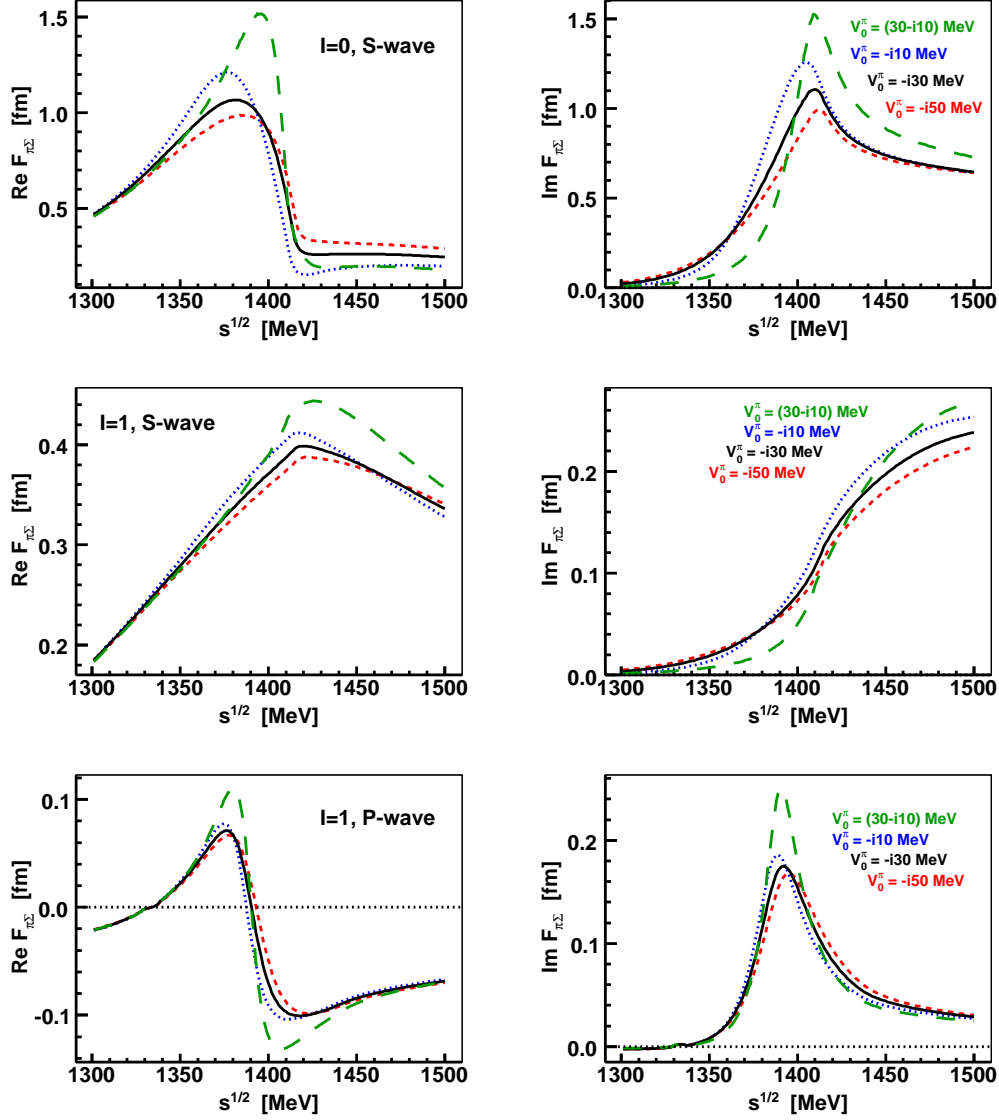


FIG. 6. A demonstration of the sensitivity of the in-medium  $\pi\Sigma$  amplitudes to a magnitude of pion absorption in nuclear matter. The dotted (blue), continuous and short-dashed (red) lines were calculated with pion-nuclear optical potential depths of  $iV_0^\pi = 10, 30$  and  $50$  MeV, respectively. For a reference the dashed (green) lines show results obtained with a pion potential adopted in Ref. [33].

First of all it is worth mentioning the narrow resonant structure above the  $K^-p$  threshold we get in the free space. The position of the peak coincides with an opening of the  $\bar{K}^0n$  channel which is also marked by a sharp dip observed in Fig. 2 for the  $\sigma(K^-p \rightarrow \pi^-\Sigma^+)$  cross section. The  $\gamma_p$  peak is related to a difference in decomposition of the two charged  $\pi\Sigma$

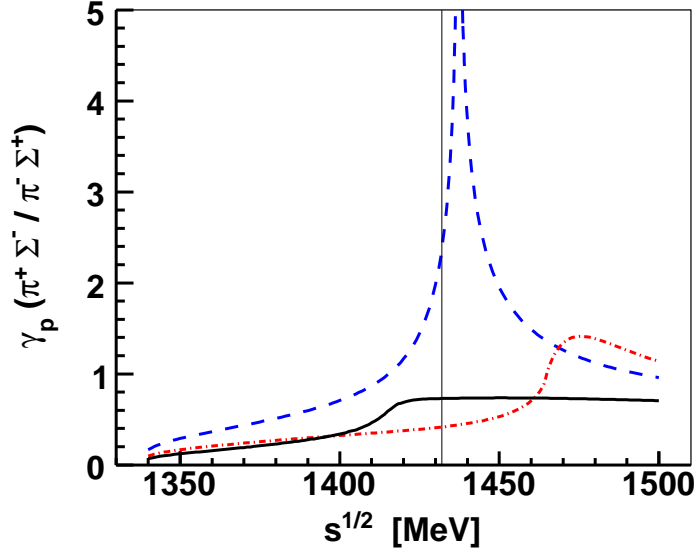


FIG. 7. Energy dependence of the branching ratio  $\gamma_p = \Gamma(\pi^+\Sigma^-)/\Gamma(\pi^-\Sigma^+)$ . The dashed (blue) line shows the free space results, the dot-dashed (red) and continuous lines demonstrate the effects of including Pauli blocking only and Pauli blocking together with hadron selfenergies, respectively. The thin vertical line marks the  $K^-p$  threshold.

states into parts with a specific isospin,

$$|\pi^-\Sigma^+\rangle = -\sqrt{\frac{1}{3}}|\pi\Sigma\rangle_{I=0} + \sqrt{\frac{1}{2}}|\pi\Sigma\rangle_{I=1} - \sqrt{\frac{1}{6}}|\pi\Sigma\rangle_{I=2} \quad (25)$$

$$|\pi^+\Sigma^-\rangle = -\sqrt{\frac{1}{3}}|\pi\Sigma\rangle_{I=0} - \sqrt{\frac{1}{2}}|\pi\Sigma\rangle_{I=1} - \sqrt{\frac{1}{6}}|\pi\Sigma\rangle_{I=2}. \quad (26)$$

Only the isoscalar and isovector parts contribute to reactions with  $K^-p$  in the initial state and the discussed branching ratio can be written as

$$\gamma_p = \frac{|T_0 + \sqrt{\frac{3}{2}}T_1|^2}{|T_0 - \sqrt{\frac{3}{2}}T_1|^2}, \quad (27)$$

where we introduced the isoscalar and isovector transition amplitudes  $T_{I=0,1} = \langle\pi\Sigma|T|\bar{K}N\rangle_{I=0,1}$ . The strong energy dependence of  $T_0$  (an partly of the  $T_1$  amplitude too) close to the  $\bar{K}N$  threshold then leads to a narrow peak at energies where the amplitudes  $T_0$  and  $T_1$  combine in such a way that the denominator of Eq. (27) becomes small, i.e. when it holds

$$\left|T_0 - \sqrt{\frac{3}{2}}T_1\right| \ll \left|T_0 + \sqrt{\frac{3}{2}}T_1\right|. \quad (28)$$

In nuclear matter this condition is not satisfied, so the peak gets dissolved. Though, one still observes a shift of the structure related to  $\Lambda(1405)$  dynamics when the Pauli blocking and hadron selfenergies are accounted for.

The strong energy dependence of the  $\gamma_p$  ratio makes its experimental value at the  $\bar{K}N$  threshold quite useful in fixing the parameters of any model that aims at a reliable qualitative description of meson-baryon interactions in that energy region. We also mention that a similar branching ratio for processes on neutron,  $\gamma_n = \sigma(K^-n \rightarrow \pi^0\Sigma^-)/\sigma(K^-n \rightarrow \pi^-\Sigma^0)$ , is not so interesting as both cross sections are composed of only the isovector transition amplitudes, so there is no  $T_0$  versus  $T_1$  interference and the rate is compatible with one in the whole energy region.

For a reference we also show the energy dependence of the other two branching ratios used in fits of the  $K^-p$  experimental data. They are given in Fig. 8 where the impact of nuclear medium on the ratios is demonstrated as well as their energy dependence. Although the opening of the  $\bar{K}^0n$  channel has a significant impact on both branching ratios the scale of variations is much smaller than in the  $\gamma_p$  case. This seems natural as the energy dependence of the probabilities present in the nominator and denominator is similar and to a large extent cancels out for both rates represented by the  $R_c$  and  $R_n$  branching ratios. It is interesting that the nuclear medium does not affect much the threshold values of both rates despite having an observable effect on their energy dependence, particularly in the  $R_n$  case.

Finally, we look at the impact of nuclear medium on the shape of the  $\pi\Sigma$  mass distributions. In Fig. 9 we present the mass distribution generated for the  $K^-p \rightarrow \pi^0\Sigma^0$  reaction. In the free space the peak is located approximately at 1420 MeV since the initial  $K^-p$  channel couples more strongly to the higher (in terms of  $\Re z$ ) of the two poles assigned to the  $\Lambda(1405)$ . The contribution of the lower pole and its distance from the real axis make the peak quite broad and clearly different from a Gaussian form. As we have already discussed the Pauli blocking moves the resonant structure to higher energies and the inclusion of hadron selfenergies moves it back to about its free-space position. Additionally, the in-medium peak is narrower and resembles more a typical Breit-Wigner distribution. We also note that a larger imaginary part of the pion selfenergy would make the in-medium peak lower and slightly broader than the one computed for  $iV_0^\pi = 30$  MeV and vice versa. Thus, the situation is similar to the one discussed in Fig. 6 and the exact shape of the in-medium  $\pi\Sigma$  mass distribution depends to some extent on the strength of pion absorption in nuclear matter.

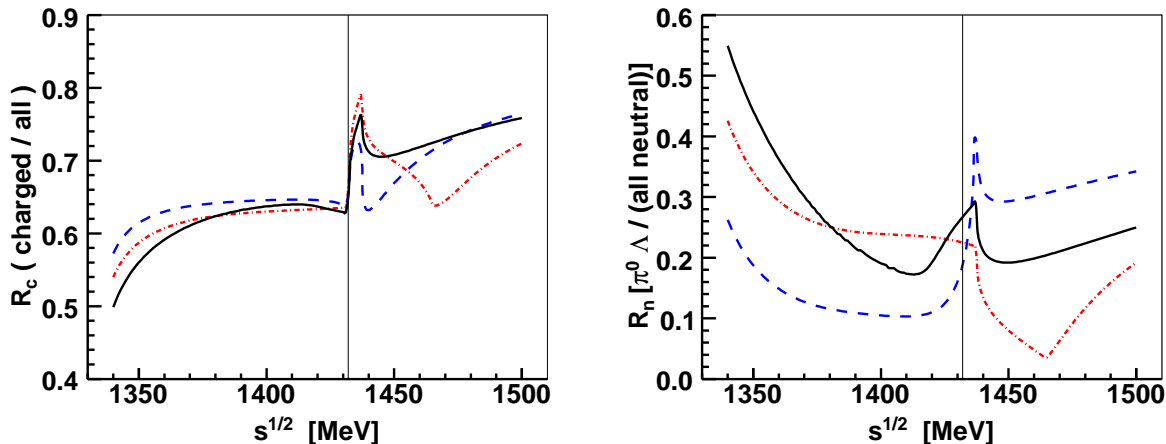


FIG. 8. Energy dependence of the branching ratios  $R_c = \Gamma(\text{charged particles})/\Gamma(\text{all})$  (left panel) and  $R_n = \Gamma(\pi^0\Lambda)/\Gamma(\text{all neutral states})$  (right panel). The dashed (blue) line shows the free space results, the dot-dashed (red) and continuous lines demonstrate the effects of including Pauli blocking only and Pauli blocking together with hadron selfenergies, respectively. The thin vertical line marks the  $K^-p$  threshold.

## V. CONCLUSIONS

We have presented a simplified model of meson-baryon interactions that is motivated by a chiral symmetry and large  $N_c$  properties of QCD. It describes quite well the  $S$ -wave and  $P$ -wave experimental data from low energy  $K^-p$  reactions. We have concentrated on implementing only the major driving forces of the meson-baryon interactions at energies around the  $\pi\Sigma$  and  $\bar{K}N$  thresholds, the leading order Tomozawa-Weinberg interaction and the direct formation of  $\Sigma(1385)$  in the  $s$ -channel for the  $S$ -wave and  $P$ -wave interactions, respectively. We believe the simplicity of the model makes it suitable to study the effects caused by nuclear medium, particularly on the shape of the resonant  $\pi\Sigma$  mass distributions that can be observed not only in the free space but in nuclear reactions as well. Understandably, the inclusion of NLO contributions in the meson-baryon interaction kernel as well as consideration of other  $P$ -wave mechanisms may alter our results to some extent. However, this would also add to a complexity of the theoretical model and most likely increase the ambiguity of its results. Still, there are opportunities for further development following this direction in the future. We also note that processes not accounted for in the two-body meson-baryon framework represent additional theoretical limitations of the model. Particu-

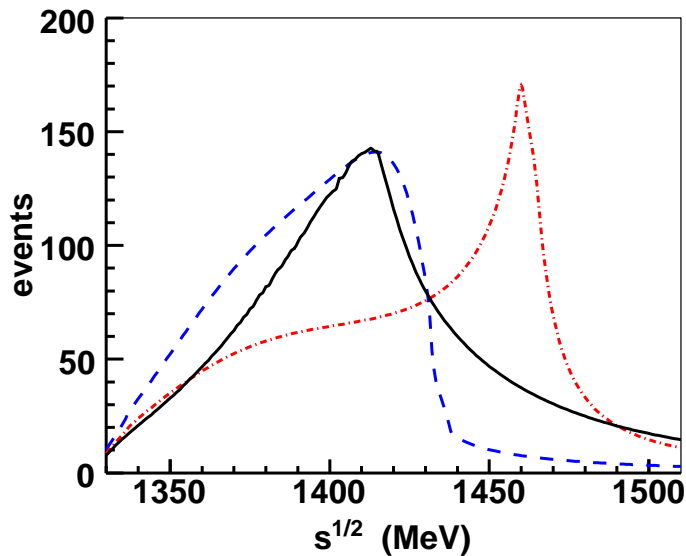


FIG. 9.  $\pi\Sigma$  mass distribution for the reaction  $K^-p \rightarrow \pi^0\Sigma^0$ . The dashed (blue) lines show the free space results, the dot-dashed (red) and continuous lines demonstrate the effects of including Pauli blocking only and Pauli blocking together with hadron selfenergies, respectively.

larly, one should anticipate slightly larger widths of the  $\Lambda(1405)$  and  $\Sigma(1385)$  resonances due to their decays into channels not included in the model or due to a larger than the adopted pion absorption in nuclear matter.

The energy and density dependence of  $\gamma_p$  shown in Fig. 7 can serve as a first step in understanding the observed results of the  $\pi^-\Sigma^+$  to  $\pi^+\Sigma^-$  formation rates reported for hypernuclear decays by the FINUDA collaboration [61]. The  $\gamma_p$  and  $\gamma_n$  branching ratios are also relevant for an analysis of data on  $K^-$  interactions with light nuclear targets that are measured by the AMADEUS collaboration in Frascati [62]. Evidently, a proper approach to these reactions is a more complex matter that requires a realistic treatment of the process dynamics as well as of the nuclear structure.

### *Acknowledgments*

We acknowledge a discussion with E. Friedman and A. Gal on the pion-nuclear optical potential. The work of A. C. was supported by the Grant Agency of the Czech Republic, Grant No. 15-04301S. V. K. is supported by RIKEN programs for junior scientists.

## APPENDIX — $SU(3)$ CLEBSCH-GORDAN COEFFICIENTS AND COUPLING MATRICES

The “meson + baryon  $\rightarrow$  baryon” interaction vertex of Eq. (15) is determined (in the leading order) by two sets of Clebsch-Gordan coefficients:  $SU(2)$  – spin determining the spin-angular momentum transition, and  $SU(3)$ -flavor determining baryon type transition. The  $SU(3)$ -flavor part is discussed here, the details of the  $SU(2)$  – spin can be found, for example, in Ref. [45].

From the group theory viewpoint, the interaction of octet meson with octet baryon can be represented as a direct product of two octet representations. The key task is to find the decomposition of this product into irreducible representations. The standard result is

$$\mathbf{8} \otimes \mathbf{8} = \mathbf{1} \oplus \mathbf{8} \oplus \mathbf{8} \oplus \mathbf{10} \oplus \overline{\mathbf{10}} \oplus \mathbf{27} . \quad (29)$$

One sees that there are two possibilities how to obtain an octet representation in the decomposition — this fact translates into the existence of two independent coefficients  $D$  and  $F$  in the conventional  $SU(3)$  chiral perturbation theory (where only octet baryons are considered). On the other hand, there is just one decuplet representation in the decomposition of Eq. (29). In principle, each transition carries an independent coupling constant — for now, let us label them  $d_8$ ,  $f_8$ , and  $g_{10}$  for the two octet and one decuplet representations, respectively. The absolute values of  $d_8$  and  $f_8$  are determined by comparison to experiment (or to conventional  $\chi$ Pt). In order to determine  $g_{10}$  we follow the large  $N_c$  limit of QCD and its consistency relations stating that pion-nucleon scattering amplitude must vanish in the leading order of the  $1/N_c$  expansion. Then, the corresponding values are:

$$d_8 \rightarrow \sqrt{\frac{5}{3}}D , \quad (30)$$

$$f_8 \rightarrow \sqrt{3}F , \quad (31)$$

$$(g_{10})^2 \rightarrow \frac{3}{4}\sqrt{\frac{2}{5}}(D + F)^2 = \frac{3}{4}\sqrt{\frac{2}{5}}(g_A)^2 . \quad (32)$$

The individual Clebsch-Gordan coefficients relevant for our model are summarized in Table I. The inverse Clebsch-Gordan coefficient (corresponding to the decuplet-octet transition) is related to the original one through a symmetry coefficient  $(-2/\sqrt{5})$ . The coupling matrix  $\mathcal{C}_{\Sigma^*0}^{d_{10}}$  determining the inter-channel coupling is shown in Table II.



TABLE I. Clebsch-Gordan coefficients for the octet-decuplet transition (baryon+meson to  $\Sigma^{*0}$ ).

$\pi^0\Lambda$	$\pi^0\Sigma^0$	$\pi^-\Sigma^+$	$\pi^+\Sigma^-$	$K^-p$	$\bar{K}^0n$	$\eta\Lambda$	$\eta\Sigma^0$	$K^0\Xi^0$	$K^+\Xi^-$
$-\frac{1}{2}$	0	$-\frac{1}{2\sqrt{3}}$	$\frac{1}{2\sqrt{3}}$	$\frac{1}{2\sqrt{3}}$	$-\frac{1}{2\sqrt{3}}$	0	$\frac{1}{2}$	$\frac{1}{2\sqrt{3}}$	$-\frac{1}{2\sqrt{3}}$

TABLE II. Coupling matrix for the  $P$ -wave interaction  $\mathcal{C}_{\Sigma^{*0}}^{d10}$ .

	$\pi^0\Lambda$	$\pi^0\Sigma^0$	$\pi^-\Sigma^+$	$\pi^+\Sigma^-$	$K^-p$	$\bar{K}^0n$	$\eta\Lambda$	$\eta\Sigma^0$	$K^0\Xi^0$	$K^+\Xi^-$
$\pi^0\Lambda$	$-\frac{3g_A^2}{8\sqrt{2}}$	0	$-\frac{1}{8}\sqrt{\frac{3}{2}}g_A^2$	$\frac{1}{8}\sqrt{\frac{3}{2}}g_A^2$	$\frac{1}{8}\sqrt{\frac{3}{2}}g_A^2$	$-\frac{1}{8}\sqrt{\frac{3}{2}}g_A^2$	0	$\frac{3g_A^2}{8\sqrt{2}}$	$\frac{1}{8}\sqrt{\frac{3}{2}}g_A^2$	$-\frac{1}{8}\sqrt{\frac{3}{2}}g_A^2$
$\pi^0\Sigma^0$		0	0	0	0	0	0	0	0	0
$\pi^-\Sigma^+$			$-\frac{g_A^2}{8\sqrt{2}}$	$\frac{g_A^2}{8\sqrt{2}}$	$\frac{g_A^2}{8\sqrt{2}}$	$-\frac{g_A^2}{8\sqrt{2}}$	0	$\frac{1}{8}\sqrt{\frac{3}{2}}g_A^2$	$\frac{g_A^2}{8\sqrt{2}}$	$-\frac{g_A^2}{8\sqrt{2}}$
$\pi^+\Sigma^-$				$-\frac{g_A^2}{8\sqrt{2}}$	$-\frac{g_A^2}{8\sqrt{2}}$	$\frac{g_A^2}{8\sqrt{2}}$	0	$-\frac{1}{8}\sqrt{\frac{3}{2}}g_A^2$	$-\frac{g_A^2}{8\sqrt{2}}$	$\frac{g_A^2}{8\sqrt{2}}$
$K^-p$					$-\frac{g_A^2}{8\sqrt{2}}$	$\frac{g_A^2}{8\sqrt{2}}$	0	$-\frac{1}{8}\sqrt{\frac{3}{2}}g_A^2$	$-\frac{g_A^2}{8\sqrt{2}}$	$\frac{g_A^2}{8\sqrt{2}}$
$\bar{K}^0n$						$-\frac{g_A^2}{8\sqrt{2}}$	0	$\frac{1}{8}\sqrt{\frac{3}{2}}g_A^2$	$\frac{g_A^2}{8\sqrt{2}}$	$-\frac{g_A^2}{8\sqrt{2}}$
$\eta\Lambda$							0	0	0	0
$\eta\Sigma^0$								$-\frac{3g_A^2}{8\sqrt{2}}$	$-\frac{1}{8}\sqrt{\frac{3}{2}}g_A^2$	$\frac{1}{8}\sqrt{\frac{3}{2}}g_A^2$
$K^0\Xi^0$									$-\frac{g_A^2}{8\sqrt{2}}$	$\frac{g_A^2}{8\sqrt{2}}$
$K^+\Xi^-$										$-\frac{g_A^2}{8\sqrt{2}}$

- 
- [1] S. Weinberg, *Physica* 96A (1979) 327–340.
- [2] J. Gasser, H. Leutwyler, *Nucl. Phys. B* 250 (1985) 465.
- [3] N. Kaiser, P. B. Siegel, W. Weise, *Nucl. Phys. A* 594 (1995) 325–345.
- [4] E. Oset and A. Ramos, *Nucl. Phys. A* 635 (1998) 99.
- [5] S. Maeda, Y. Akaishi, T. Yamazaki, *Proc. Jpn. Acad., B* 89 (2013) 418–437.
- [6] J. Mareš, E. Friedman, A. Gal, *Nucl. Phys. A* 770 (2006) 84.
- [7] D. Gazda, J. Mareš, *Nucl. Phys. A* 881 (2012) 159.
- [8] J. Schaffner-Bielich, S. Schramm, H. Stöcker, *Proc. Intl. School of Physics Enrico Fermi, Course CLXVII*, Eds. M. Anselmino *et al.* (IOS Press, Amsterdam, 2008) 119144.
- [9] G. t’Hooft, *Nucl. Phys. B* 72 (1974) 461.

- [10] E. Witten, Nucl. Phys. B 160 (1979) 57.
- [11] J.L. Gervais, B. Sakita, Phys. Rev. Lett. 52 (1984) 87.
- [12] R.F. Dashen, A.V. Manohar, Phys. Lett. B 513 (1993) 425.
- [13] T. Hyodo, D. Jido, Prog. Part. Nucl. Phys. 67 (2012) 55–98.
- [14] T. Hyodo, W. Weise, Phys. Rev. C 77 (2008) 035204.
- [15] J. A. Oller, U.-G. Meißner, Phys. Lett. B 500 (2001) 263–272.
- [16] D. Jido, J. A. Oller, E. Oset, A. Ramos, U.-G. Meißner, Nucl. Phys. A 725 (2003) 181–200.
- [17] G. Agakishievet *et al.* [HADES Collaboration], Phys. Rev. C 87 (2013) 025201.
- [18] I. Zychor *et al.* [ANKE Collaboration], Phys. Lett. B 660 (2008) 167–171.
- [19] R. J. Hemingway, Nucl. Phys. B 253 (1985) 742–752.
- [20] K. Moriya *et al.* [CLAS Collaboration], Phys. Rev. C 88 (2013) 045201.
- [21] L. Roca, E. Oset, Phys. Rev. C 87, 055201 (2013).
- [22] M. Mai, U.-G. Meißner, Eur. Phys. J. A 51, 30 (2015).
- [23] A. Scordo *et al.* [AMADEUS Collaboration], arXiv:1304.7149 [nucl-ex].
- [24] B. Borasoy, R. Nißler, W. Weise, Eur. Phys. J. A 25 (2005) 79–96.
- [25] A. Cieplý, J. Smejkal, Nucl. Phys. A 881 (2012) 115–126.
- [26] Y. Ikeda, T. Hyodo, W. Weise, Nucl. Phys. A 881 (2012) 98–114.
- [27] Z.-H. Guo, J. Oller, Phys. Rev. C 87 (2013) 035202.
- [28] T. Waas, N. Kaiser, W. Weise, Phys. Lett. B 365 (1996) 12–16.
- [29] M. Lutz, Phys. Lett. B 426 (1998) 12–20.
- [30] A. Ramos, E. Oset, Nucl. Phys. A 671 (2000) 481–502.
- [31] A. Cieplý, E. Friedman, A. Gal, J. Mareš, Nucl. Phys. A 696 (2001) 173–193.
- [32] L. Tolós, A. Ramos, E. Oset, Phys. Rev. C 74, 015203 (2006).
- [33] A. Cieplý, E. Friedman, A. Gal, D. Gazda, J. Mareš, Phys. Rev. C 84 (2011) 045206.
- [34] E. Friedman, A. Gal, C. J. Batty, Nucl. Phys. A 579 (1994) 518–538.
- [35] E. Friedman, A. Gal, Nucl. Phys. A 899 (2013) 60.
- [36] D. Jido, E. Oset, A. Ramos, Phys. Rev. C 66 (2002) 055203.
- [37] V. Krejčířík, Phys. Rev. C 86 (2012) 024003.
- [38] M.L. Goldberger, K.M. Watson, *Collision theory*, John Willey & Sons (1964).
- [39] Y. Yamaguchi, Phys. Rev. 95 (1954) 1628.
- [40] Y. Yamaguchi, Y. Yamaguchi, Phys. Rev. 95 (1954) 1635.

- [41] J.L. Gervais, B. Sakita, Phys. Rev. D 30 (1984) 1795.
- [42] R.F. Dashen, A.V. Manohar, Phys. Lett. B 513 (1993) 438.
- [43] R.F. Dashen, E.E. Jenkins, A.V. Manohar, Phys. Rev. D 49 (1994) 4713.
- [44] R.F. Dashen, E.E. Jenkins, A.V. Manohar, Phys. Rev. D 51 (1995) 3697.
- [45] T.D. Cohen, V. Krejčířk, Phys. Rev. C 85 (2012) 035205.
- [46] J.J. de Swart, Rev. Mod. Phys. 35 (1963) 16.
- [47] T.D. Cohen, R.F. Lebed, Phys. Rev. D 70 (2004) 096015.
- [48] A. Cieplý, E. Friedman, A. Gal, J. Mareš, Nucl. Phys. **A925** 126 (2014).
- [49] M. B. Johnson, G. R. Satchler, Ann. Phys. 248, 134 (1996).
- [50] Center of Nuclear Study Data Analysis Center, URL: <http://gwdac.phys.gwu.edu/KWW>.
- [51] E. Friedman, Phys. Rev. C 28, 1264 (1983).
- [52] J. Ciborowski *et al.*, J. Phys. G 8 (1982) 13.
- [53] D. Evans *et al.*, J. Phys. G 9 (1983) 885.
- [54] M. Sakitt *et al.*, Phys. Rev. 139 (1965) 719.
- [55] W.E. Humphrey, R.R. Ross, Phys. Rev. 127 (1962) 1305.
- [56] T.S. Mast *et al.*, Phys. Rev. D 14 (1976) 13.
- [57] R.O. Bangerter *et al.*, Phys. Rev. D 23 (1981) 1485.
- [58] M.B. Watson, M. Ferro-Luzzi, R.D. Tripp, Phys. Rev. 131 (1963) 2248.
- [59] K.A. Olive *et al.* (Particle Data Group), Chin. Phys. C 38, 090001 (2014).
- [60] A.D. Martin, Nucl. Phys. B 179 (1981) 33.
- [61] M. Agnelo *et al.* [FINUDA Collaboration], Phys. Lett. B 704 (2011) 474-480.
- [62] K. Piscicchia *et al.* [AMADEUS Collaboration], PoS Bormio2013 (2013) 034, arXiv:13044.7165 [nucl-ex].